Indian Journal of Chemistry
Vol. 55A, February 2016, pp. 153-159

Humic acid-induced synthesis of hierarchical basic copper carbonate/AlOOH microspheres and its enhanced catalytic activity for 4-nitrophenol reduction

Wenjin Zhang, Zhengbin Tian, Lijian Chen & Shiyun Ai*

College of Chemistry and Material Science, Shandong Agricultural University, Taian, 271018, PR China

Email: ashy@sdau.edu.cn

Received 7 July 2015; revised and accepted 15 January 2016

One-pot synthesis of basic copper carbonate/AlOOH microspheres with hierarchical structure in the absence and presence of humic acid is presented. The synthesized microspheres are characterized by SEM, EDS, TEM, XRD, FT-IR and TGA data. The catalytic ability of these hierarchical structures has been evaluated with reduction of 4-nitrophenol to 4-aminophenol with excess amount of $NaBH_4$ as a model reaction. The reduction is regarded as a pseudo first-order reaction and the activation energy calculated to from the Arrhenius plots. The urchin-like HA-BBC/AlOOH shows better catalytic performance than the pure BBC/AlOOH samples with flower-like structure.

Keywords: Catalysts, Reduction, Nitrophenol reduction, Microspheres, BCC/AlOOH microspheres, Humic acid, Hierarchical structure

Cu^{2+} ion, as one of the heavy metal ions, is poisonous to environment. Therefore, conversion of Cu^{2+} ion into copper catalysts is significant. For instance, Cu-containing hydrotalcites are useful as catalysts or catalyst precursors due to their large surface area, high catalytic activity, good thermal stability, and environmentally friendly[1, 2] and have attracted great attention and been widely applied[3-6]. However, the Cu-containing hydrotalcites are difficult to the synthesis due to the Jahn-Teller distortion[7,8]. Consequently, much effort has been made to prepare hydrotalcites containing copper for different purposes[9, 10]. Moreover, an increasing number of other Cu-containing catalysts are being researched and applied, such as Cu_2O[11], CuO[12], Cu-M (M: other metals) mixed oxides[2, 13, 14], and Cu-based alloys[15].

The principal component of humic substances humic acid (HA) is soluble in dilute alkali solution but insoluble in the solution of *p*H < 6.5 (ref. 16). A variety of organic functional groups, notably carboxylate and phenolate groups endows HA the ability of absorbing metal ions such as Mg^{2+}, Ca^{2+}, Cu^{2+}, Fe^{3+}, Al^{3+} (ref. 17). Pandey *et al.*[18] studied the stability of metal-humic acid complexes and their crucial role in environmental detoxification. Tan *et al.*[19] reported that humic acid is capable of detoxifying lakes affected by metal pollution due to its enormous chelation capacity[19]. Furthermore, the influence of humic acid on the aggregation kinetics of carbon materials, such as fullerene nanoparticles[20] and single-walled carbon nanotubes has also been studied[21]. In recent years, there has been an increasing interest in the synthesis of nanoparticles in the presence of humic substances as a novel cheap and green template. Akaighe *et al.*[22] reported the formation of humic acid-induced silver nanoparticle under environmentally relevant conditions, while Polyakov *et al.*[23] investigated the constrained growth of anisotropic magnetic δ-FeOOH nanoparticles in the template of humic substances.

CuAl hydrotalcites with large surface area were expected to be produced in the presence of humic acid. However, hierarchical basic copper carbonate/AlOOH (BCC/AlOOH) microspheres were obtained under our experimental conditions. Nitrophenol reduction is presently considered as a benchmark reaction to test a catalyst nanoparticle[24]. To our surprise, the hierarchical microspheres exhibited excellent catalytic ability for 4-nitrophenol reduction with sodium borohydride. In the present work, we compare the morphology and catalytic ability of two microspheres, formed in the absence and presence of humic acid as template. We report a direct experimental evidence of the template role of humic acid in the synthesis of BCC/AlOOH microspheres. In addition, the results reveal the stable nature and good catalytic ability of this catalyst.

Materials and Methods

$Cu(NO_3)_2{\cdot}3H_2O$, $Al(NO_3)_3{\cdot}9H_2O$, and $NaBH_4$ were purchased from Tianjin Basf Co., Ltd (China). Urea was purchased from Kay Tong Chemical Reagents Co., Ltd (Tianjin, China), while 4-nitrophenol and humic acid were purchased from Aladdin (Shanghai, China). All reagents employed were of analytical grade and used without further purification. Doubly distilled deionized water was used throughout the experiment.

Scanning electron microscopy (SEM) and energy dispersive X-ray spectroscopy (EDS) were recorded on S4800 scanning electron microscope (Japan). Transmission electron microscopy (TEM) was performed on JEM-100CX electron microscope (Japan). X-ray powder diffraction (XRD) data were collected using a Rigaku DLMAX-2550 V diffractometer (40 kV, Cu Kα; scan speed of 6°/min). UV–vis absorption spectra and kinetic measurements were recorded on a UV–2450 Shimadzu vis-spectrometer (Japan). Fourier transform infrared (FT-IR) spectra (KBr as pellet) were obtained on Thermo Nicolet-380 IR spectrophotometer (USA). Thermogravimetric analysis (TGA) was carried out on DTG-60AH Shimadzu thermogravimetric analyzer (Japan). Photographs were taken by a Canon G11 digital camera.

Basic copper carbonate/AlOOH and humic acid-induced basic copper carbonate/AlOOH microspheres were synthesized as follows: $Cu(NO_3)_2{\cdot}3H_2O$ (0.004 mol), $Al(NO)_3{\cdot}9H_2O$ (0.002 mol), urea (0.02 mol), and humic acid (0.005 g) were completely dissolved in water (80 mL) under vigorous stirring. The control experiment was carried out without humic acid. The obtained homogeneous solutions were transferred to two Teflon-lined stainless-steel autoclaves (100 mL) and sealed to heat at 100 °C for 48 h. Then, they were cooled to room temperature naturally. The resulting products were filtered, washed with ethanol and deionized water in sequence, and air-dried overnight at room temperature.

For the catalytic reduction of 4-nitrophenol (4-NP), 20 μL of 4-NP aqueous solution (0.01 *M*) was mixed with 2 mL distilled water in a quartz cell (1.0 cm path length and 4 mL volume). Subsequently, freshly prepared 500 μL aqueous solution of $NaBH_4$ (0.2 *M*) was added, resulting in a color change from light-yellow to yellow-green. Then, 20 μL of catalyst dispersion (1 mg mL^{-1}) was added to the above solution. The conversion of 4-NP to 4-AP was subsequently detected via UV–vis spectroscopy in the range of 200-600 nm.

Results and Discussion

The SEM image in Fig. 1a shows that a large quantity of microspheres are distributed randomly with size of 3–20 μm. Magnification of the SEM image (Fig. 1b) reveals the flower-like structures of the microsphere with some debris. Also, some microspheres comprised nanoflakes of irregular size (Fig. 1c). The SEM image in Fig. 1(d) clearly

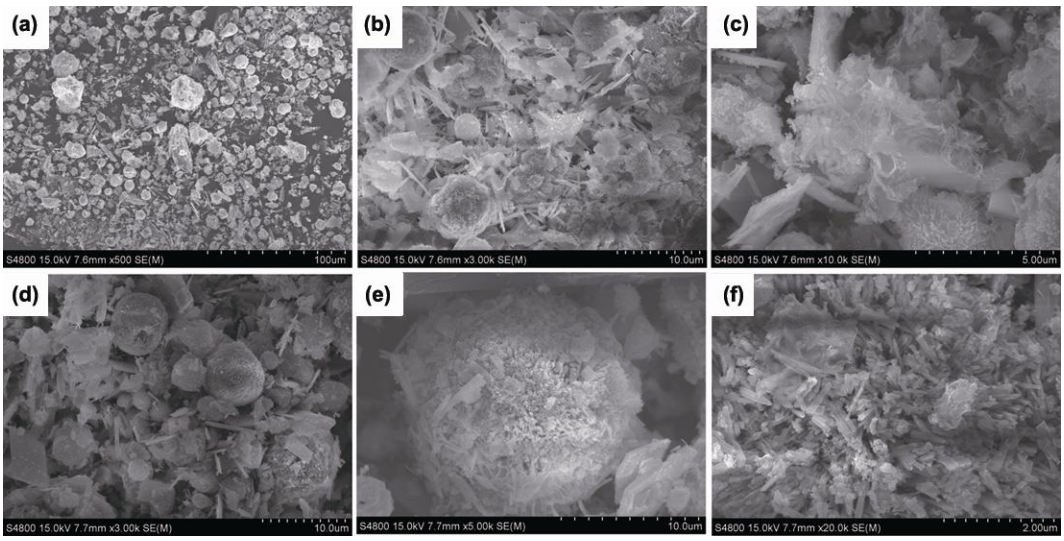

Fig. 1–SEM images of BCC/AlOOH (a, b, c) and HA-BCC/AlOOH (d, e, f) samples.

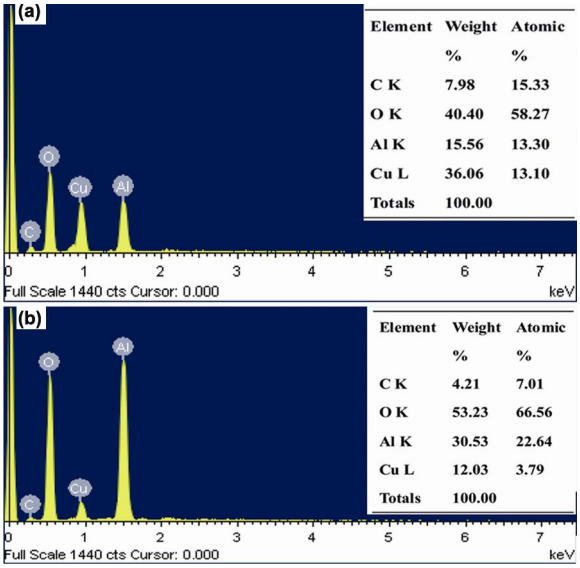

Fig. 2–EDX images of BCC/AlOOH (a) and HA-BCC/AlOOH (b) samples.

illustrates the microsphere morphology of HA-BCC/AlOOH composite with size in the range of 3–10 μm. Urchin-like morphology along with nanostrips with some kind of debris is observed on the surface of HA-BCC/AlOOH samples in the magnified SEM image (Fig. 1e). The width and length of these nanostrips are in the ranges of 5–15 and 80–120 nm, respectively.

The EDS spectrum (Fig. 2) indicates that C, O, Cu, and Al elements exist in the hierarchical BCC/AlOOH and HA-BCC/AlOOH microspheres. However, the Al content in the urchin-like HA-BCC/AlOOH structures is roughly higher than that of the flower-like BCC/AlOOH composite.

Figure 3(a) shows the XRD pattern of the as-synthesized samples. For both, almost all the diffraction peaks can be assigned to malachite $Cu_2(CO_3)(OH)_2$. Strong and narrow diffraction peaks indicate that the product is fully crystallized. It is a

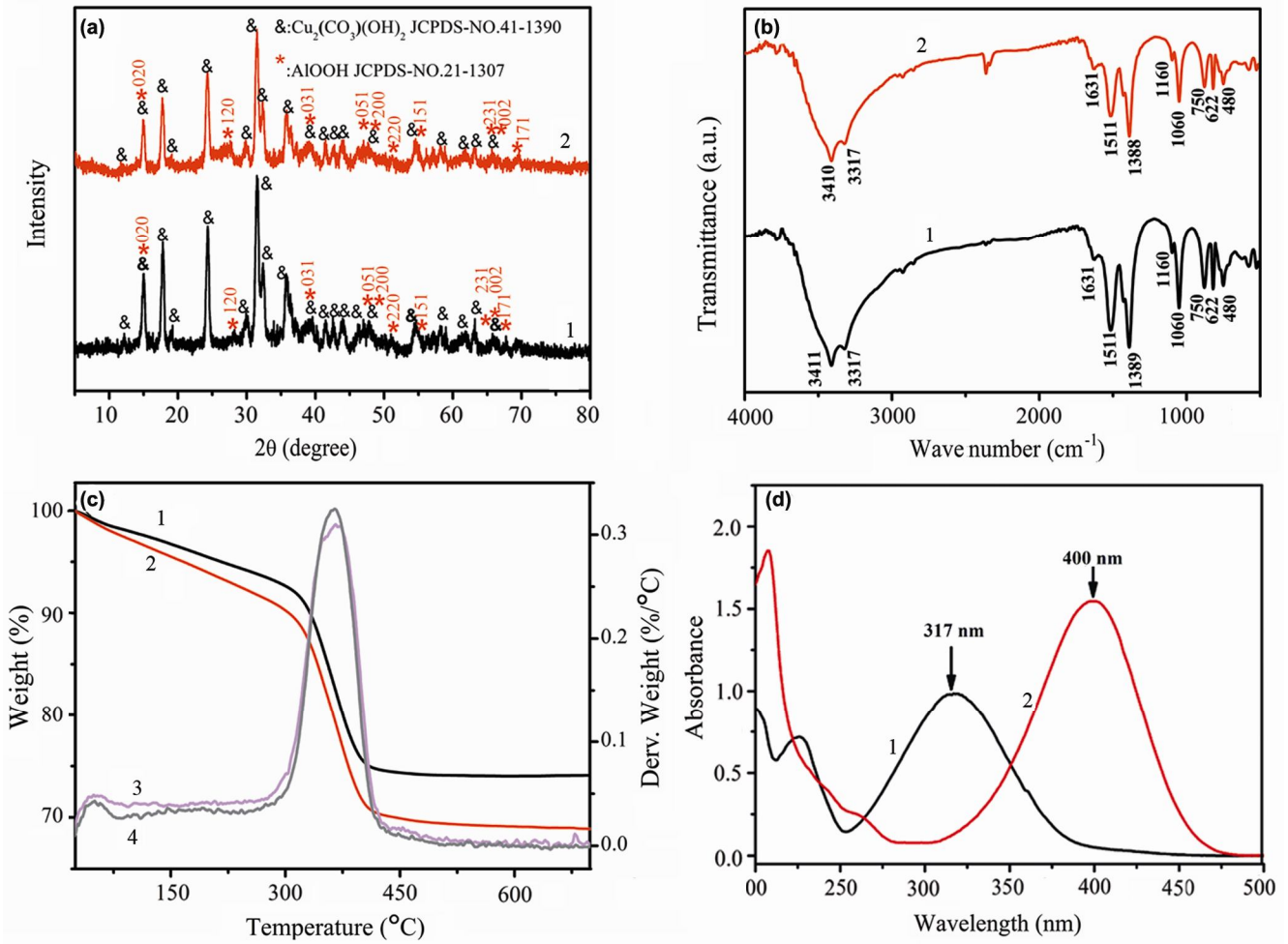

Fig. 3–(a) XRD patterns, (b) FT-IR spectra of BCC/AlOOH (1) and HA-BCC/AlOOH (2) samples, (c) TGA and DTG curves of BCC/AlOOH (1, 3) and HA-BCC/AlOOH (2, 4) composites, and, (d) UV-vis absorption spectra of 4-NP before (1) and after addition of the NaBH4 solution (2).

little difficult to identify the AlOOH phases because some diffraction peaks such as (020), (031), (051) overlaped with those of $Cu_2(CO_3)(OH)_2$. However, the characteristic peaks (120), (220), (171) of orthorhombic AlOOH can be observed. Compared with template-free BCC/AlOOH product, the intensity of diffraction peak (020) in the HA-BCC/AlOOH superstructure is lower and the intensity of peak (120) increases. This phenomenon may be caused by preferential growth along the (120) plane and closely packed structure in an ordered fashion. The decrease in the intensity of diffraction peaks also implies that the diameter of material decreases.

The FTIR spectra of BCC/AlOOH and HA-BCC/AlOOH samples show almost no difference between the two (Fig. 3(b)). There is a very strong and broad band centered at 3411 cm^{-1} with a shoulder at 3317 cm^{-1}, which were assigned to υ_{as} O-H and υ_s O-H stretching vibrations. The peak at 1630 cm^{-1} was due to the bending mode of hydroxyl groups on the surface and in the absorbed water molecules. The sharp peak at 1060 cm^{-1} with a small shoulder at 1160 cm^{-1} belongs to δ_s O-H and δ_{as} O-H modes, respectively. Three peaks at 750, 622, 480 cm^{-1} are due to the M-O stretching and bending vibration modes. These characteristic bands agree with those in the previous reports[25, 26]. The peaks at 1511 cm^{-1} and 1389 cm^{-1} (1388 cm^{-1}) are assigned to stretching and bending modes of C-O bonds, respectively.

TGA and DTG curves were plotted to explore the thermal behavior of BCC/AlOOH and HA-BCC/AlOOH samples. Two decomposition steps were observed in these samples (Fig. 3c). For BCC/AlOOH, the first step, a small and broad DTG endotherm at around 49.5 °C with a mass loss of 2.5%, is attributed to desorption of physically adsorbed water. The second and last step at about 366.7 °C with a mass loss of 30%, is consistent with CO_2 and H_2O[27]. In addition, the removal of hydroxyl bridges from the layer structure of AlOOH agrees with the theoretical value for conversion of AlOOH to Al_2O_3[28]. The TGA curve displays the beginning of decomposition of the sample at about 283 °C, while the final stage of decomposition was not complete until about 427 °C. However, there is a little difference in the case of HA-BCC/AlOOH. The first step, a mass loss of 3.8% at 50.7 °C corresponded to moisture loss. The second step, the major endothermic decomposition occurred 365.0 °C with a mass loss of 32%. This is also attributed to the CO_2 and H_2O loss. The thermogram shows that the decomposition of the composite begins at ~287 °C and the decomposition is finally complete at 438 °C. The above analysis of the two samples indicates that the BCC/AlOOH had better stability in heat than the HA-BCC/AlOOH composite.

In order to evaluate the catalytic activity of BCC/AlOOH and HA–BCC/AlOOH composites, the reduction of 4-NP to 4-aminophenol (4-AP) with an excess amount of $NaBH_4$ was employed as a benchmark model reaction[24]. Generally, 4-NP solution shows a strong absorption peak at 317 nm (Fig. 3d). Upon the addition of $NaBH_4$ solution, the absorption peak was red-shifted to 400 nm immediately, corresponding to a color change from light yellow to yellow-green, due to formation of the 4-nitrophenolate ion in alkaline environment.

The catalytic reduction of 4-NP to 4-AP over BCC/AlOOH and HA-BCC/AlOOH composites was carried out (Fig. 4). After the addition of catalysts, the

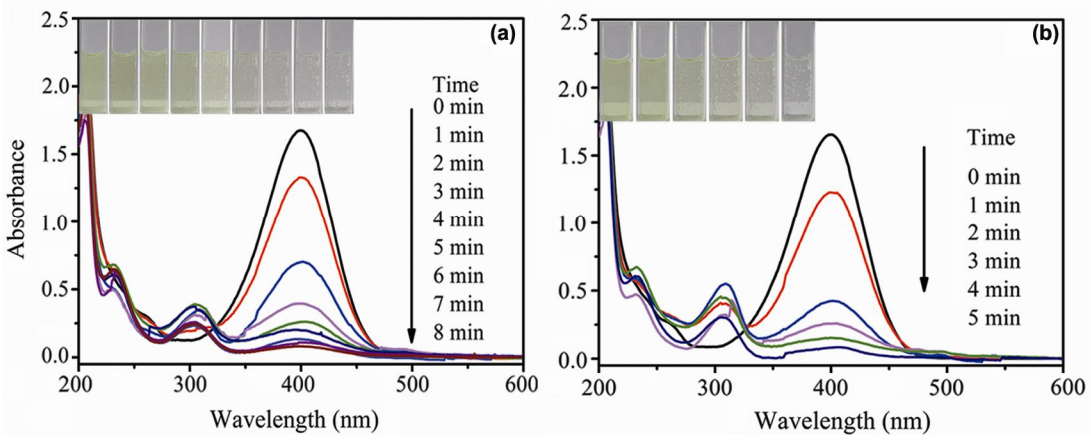

Fig. 4–UV-vis absorption spectra during the catalytic reduction of 4-NP over (a) BCC/AlOOH, and, (b) HA-BCC/AlOOH catalysts. [Inset: Successive color changes of 4-NP solutions under reduction].

maximum absorption of 4-nitrophenolate ion at 400 nm gradually decreased with the appearance of a new absorption peak at 295 nm attributed to 4-AP. Meanwhile, the color of 4-nitrophenolate ion disappeared gradually. From the absorption spectra and the color changes shown in the Fig. 4(a), it is seen that it required 8 min to catalyze the conversion of 4-NP to 4-AP over BCC/AlOOH microspheres. However, with the HA-BCC/AlOOH microsphere catalyst, the absorption peak of 4-nitrophenolate ion almost diminished completely after 5 min (Fig. 4b). Presumably, there are two main factors leading to this difference of catalytic performance. Firstly, an increase in amount of Al in HA-BCC/AlOOH composite plays an important role. AlOOH as support material of noble metal catalysts has been investigated earlier[28, 29]. In order to investigate the catalytic capacity of HA-BCCOOH and HA-BCC/AlOOH catalysts, the catalytic reduction of 4-NP to 4-AP over HA-BCCOOH catalysts was studied Fig. 5(a). After the addition of HA-BCCOOH catalysts, the absorption maximum of 4-nitrophenolate ion at 400 nm gradually decreased with a slight response from 0 min to 8 min. On increasing the time from 1 min to 3 min, the catalytic activity increased correspondingly; however, on further increase, the catalytic activity was almost the same. In Fig. 5(b), three different absorption peaks of 4-nitrophenolate ion over HA-BCCOOH and HA-BCC/AlOOH microspheres are seen. The lower catalytic capacity of HA-BCCOOH as compared to HA-BCC/AlOOH catalysts definitely testify that Al in HA-BCC/AlOOH composite plays an important role. Presumably, increased Al element content can improve the surface area of the support material of HA-BCC/AlOOH catalysts. Secondly, on synthesis in the presence of HA, the nanostrips morphology of HA-BCC/AlOOH has larger surface area than that of BCC/AlOOH samples. As a result, more reaction sites appear in the HA-BCC/AlOOH microspheres.

Since excess amount of $NaBH_4$ is used in the reaction, the reduction can be regarded as a pseudo-first order reaction on the basis of evaluation of the rate constant with regard to 4-NP only. Therefore, the reaction kinetics can be described as $\ln(C/C_0) = -kt$, where k is the apparent first-order rate constant (min^{-1}), t is the reaction time. Plots C/C_0 and $\ln(C/C_0)$ versus reaction time for the reduction of 4-NP to 4-AP over BCC/AlOOH and HA–BCC/AlOOH microspheres are shown in Fig. 6(a). It is observed that both BCC/AlOOH and HA-BCC/AlOOH composites exhibit high catalytic activities. Moreover, HA-BCC/AlOOH (0.62 min^{-1}) shows better performance than BCC/AlOOH (0.39 min^{-1}) microspheres. This indicates that the catalytic efficiency was greatly enhanced by the addition of HA in the synthesis procedure. Furthermore, the rate constant k of urchin-like HA–BCC/AlOOH catalyst obtained herein was higher than that of flower-like Au-Fe_3O_4 heterostructures (0.38 min^{-1}) (ref. 30), core-shell structured Fe_3O_4@SiO_2-Ag magnetic nanocomposite (0.46 min^{-1}) (ref. 31), thiol-stabilized $Au_{25}L_{18}$ monolayer protected clusters (0.08–0.51 min^{-1}) (ref. 32), coral-like dendrite Ag nanocrystal (0.31 min^{-1}) and banana leaves-like dendrite Ag nanocrystals (0.10 min^{-1}, 0.16 min^{-1}) (ref. 33), but was lower than that of well-dispersed silver nanoparticles on hierarchical flower-like $Ni_3Si_2O_5(OH)_4$ (0.63 min^{-1}) (ref. 34).

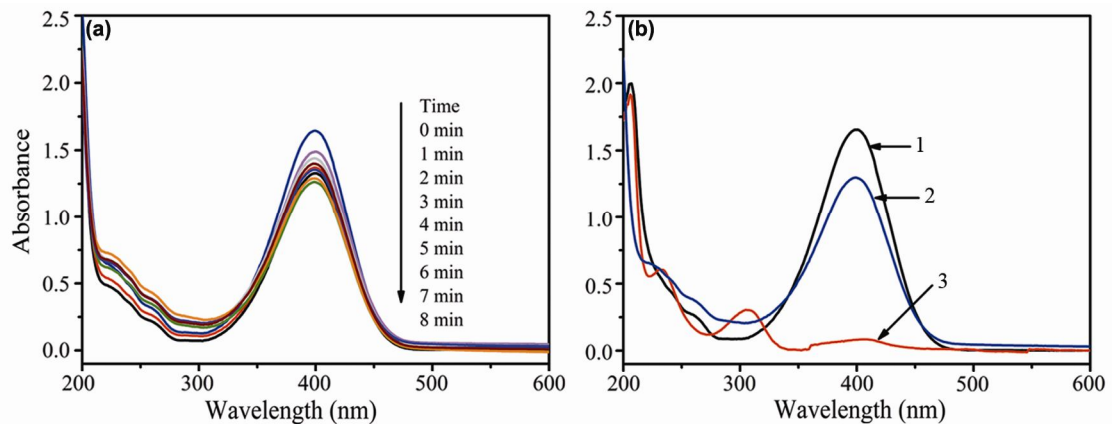

Fig. 5–(a) UV-vis absorption spectra during the catalytic reduction of 4-NP over HA-BCCOOH catalysts. (b) UV-vis absorption spectra of 4-NP reduction before (1), over HA-BCCOOH (2), and, HA-BCC/AlOOH (3) catalysts.

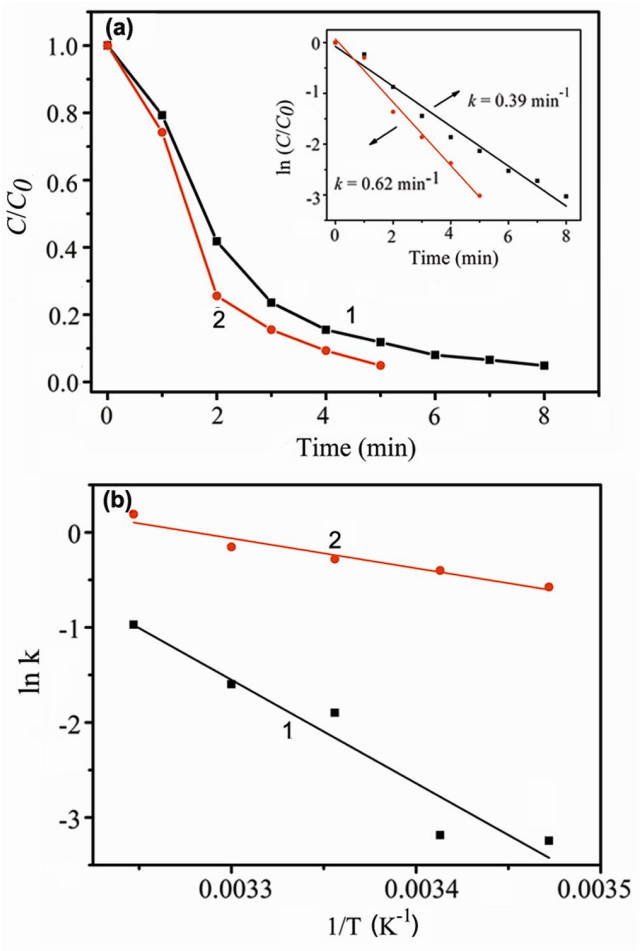

Fig. 6–(a) C/C_0 versus reaction time for the reduction of 4-NP over BCC/AlOOH (1), and, HA–BCC/AlOOH (2) catalysts. [Inset: ln(C/C_0) versus reaction time for the reduction of 4-NP over different composites. C_0 and C are the peak absorbance at 400 nm initially and at time t, respectively]. (b) Arrhenius plots of ln(k) versus 1/T under reduction of 4-NP catalyzed by BCC/AlOOH (1), and, HA-BCC/AlOOH (2) microspheres in the temperature range of 288-308 K.

The Arrhenius plots of the reaction rate constants obtained in the range of 288-308 K (Fig. 6b), was calculated to be 90 kJ mol^{-1} for flower-like BCC/AlOOH catalyst and 26 kJ mol^{-1} for the urchin-like HA-BCC/AlOOH catalyst. The value for urchin-like HA-BCC/AlOOH is relatively smaller than that of flowerlike BCC/AlOOH system, that of the mainly because the surface area of the urchin-like HA-BCC/AlOOH is larger than flower-like BCC/AlOOH microsphere. This is in good agreement with the results of previous work[35] and shows that the activation energy is greatly dependent on the surface area of catalyst.

Conclusions

In conclusion, pure BCC/AlOOH microspheres and HA-BCC/AlOOH microspheres with different hierarchical structures were synthesized. The SEM, EDS, TEM, XRD, FT-IR, TGA analyses showed the hierarchical morphology and the template influence of humic acid. The catalytic experiments revealed that urchin-like HA-BCC/AlOOH microspheres has a good catalytic capability with the apparent first-order rate constant of 0.62 min^{-1}, while that with the flower-like BCC/AlOOH microspheres was 0.39 min^{-1}. The *Ea* was 26 kJ mol^{-1} and 90 kJ mol^{-1} for the urchin-like HA-BCC/AlOOH catalyst and flower-like BCC/AlOOH catalyst respectively. The urchin-like HA-BBC/AlOOH showed better catalytic performance than the pure BBC/AlOOH samples with flower-like structure for the reduction of 4-NP to 4-AP.

Acknowledgement

This work is supported by the National Natural Science Foundation of China (no. 21375079, 21105056), PR China and Project of Development of Science and Technology of Shandong Province, PR China (No. 2013GZX20109).

References

1 Tsoncheva T, Vankova S & Mehandjiev D, *Fuel*, 82 (2003) 755.
2 Chmielarz L, ´strowski P K, Rafalska-Łasocha A, Majda D & Dziembaj R, *Appl Catal B Environ*, 35 (2002) 195.
3 Chen L, Sun K, Li P, Fan X, Sun J & Ai S, *Nanoscale*, 5 (2013) 10982.
4 Crivello M, Pérez C, Herrero E, Ghione G, Casuscelli S & Rodríguez-Castellón E, *Catal Today*, 107 (2005) 215.
5 Zhu B C & Jiang X Z, *Appl Organomet Chem*, 21 (2007) 345.
6 Alejandre A, Medina F, Salagre P, Correig X & Sueiras J E, *Chem Mater*, 11 (1999) 939.
7 Shannon R D, *Acta Cryst*, A 32 (1976) 751.
8 Tsoncheva T, Vankova S & Mehandjiev D, *Physica B*, 373 (2006) 267.
9 Corma A, Palomares A E, Rey F & ´arquez F M, *J Catal*, 170 (1997) 140.
10 Rives V & Kannan S, *J Mater Chem*, 10 (2000) 489.
11 Jongh P E d, Vanmaekelbergh D & Kelly J J, *Chem Commun*, (1999) 1069.
12 Chen W, Hong L, Liu A L, Liu J Q, Lin X H & Xia X H, *Talanta*, 99 (2012) 643.
13 Li Z, Fan H, Zheng H & Liu Y, *Chinese J Catal*, 31 (2010) 471.
14 Pradhan N, Pal A & Pal T, *Langmuir*, 17 (2001) 1800.
15 Zhou S, Varughese B, Eichhorn B, Jackson G & McIlwrath K, *Angew Chem*, 117 (2005) 4615.
16 Kerndorff H & Schnitzer M, *Geochim Cosmochim Acta*, 44 (1980) 1701.
17 Kinniburgh D G, Milne C J, Benedetti M F, Pinherio J P, Filius J, Koopal L K & Riemsdijk W H V, *Environ Sci Technol*, 30 (1996) 1687.

18 Pandey A K, Pandey S D & Misra V, *Ecotoxicol Environ Safety*, 47 (2000) 195.

19 Chen L, Sun B, Wang X, Qiao F & Ai S, *J Mater Chem B*, 1 (2013) 2268.

20 Chen K L & Elimelech M, *J Colloid Interface Sci*, 309 (2007) 126.

21 Saleh N B, Pfefferle L D & Elimelech M, *Environ Sci Technol*, 44 (2010) 2412.

22 Akaighe N, Maccuspie R I, Navarro D A, Aga D S, Banerjee S, Sohn M & Sharma V K, *Environ Sci Technol*, 45 (2011) 3895.

23 Polyakov A Y, Goldt A E, Sorkina T A, Perminova I V, Pankratov D A, Goodilin E A & Tretyakov Y D, *CrystEngComm*, 14 (2012) 8097.

24 Aditya T, Pal A & Pal T, *Chem Commun*, 51 (2015) 9410.

25 Feng Y, Lu W, Zhang L, Bao X, Yue B, Lv Y & Shang X, *Cryst Growth Des*, 8 (2008) 1426.

26 Zhang J, Liu S, Lin J, Song H, Luo J, Elssfah E M, Ammar E, Huang Y, Ding X, Gao J, Qi S & Tang C, *J Phys Chem B*, 110 (2006) 14249.

27 Pourmortazavi S M, Kohsari I & Hajimirsadeghi S S, *Cent Eur J Chem*, 7 (2008) 74.

28 Zhou Y, Fu H, Zheng X, Li R, Chen H & Li X, *Catal Commun*, 11 (2009) 137.

29 Doskocil E & Mueller G, *J Catal*, 234 (2005) 143.

30 Lin F-h & Doong R-a, *J Phys Chem C*, 115 (2011) 6591.

31 Chi Y, Yuan Q, Li Y, Tu J, Zhao L, Li N & Li X, *J Colloid Interface Sci*, 383 (2012) 96.

32 Shivhare A, Ambrose S J, Zhang H, Purves R W & Scott R W, *Chem Commun*, 49 (2013) 276.

33 Rashid M H & Mandal T K, *J Phys Chem C*, 111 (2007) 16750.

34 Jin R, Xing Y, Yu X, Sun S, Yu D, Wang F, Wu W & Song S, *Chem: Asian J*, 7 (2012) 2955.

35 Panigrahi S, Basu S, Praharaj S, Pande S, Jana S, Pal A, Ghosh S K & Pal T, *J Phys Chem C*, 111 (2007) 4596.